Heliyon 9 (2023) e20975

Contents lists available at ScienceDirect

Heliyon

journal homepage: www.cell.com/heliyon

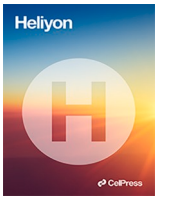

Nanocomposite based on Gd_2O_3 nanoparticles and drug 5-fluorouracil as potential theranostic nano-cargo system

Jaroslava Szűcsová [a], Adriana Zeleňáková [a,*], Eva Beňová [b], Ľuboš Nagy [a], Martin Orendáč [a,d], Veronika Huntošová [c], Mária Šoltésová [e], Jaroslav Kohout [e], Vít Herynek [f], Vladimír Zeleňák [b]

[a] Institute of Physics, P. J. Šafárik University, Park Angelinum 9, 040 01 Kosice, Slovakia
[b] Institute of Chemistry, P. J. Šafárik University, Moyzesova 11, 040 01 Kosice, Slovakia
[c] Center for Interdisciplinary Biosciences, P. J. Šafárik University, Jesenná 5, 040 01 Kosice, Slovakia
[d] Department of Solid State Engineering, University of Chemistry & Technology, Technická 5, 166 28 Prague, Czech Republic
[e] Department of Low Temperature Physics, Faculty of Mathematics and Physics, Charles University, V Holešovičkách 2, 182 00 Prague, Czech Republic
[f] First Faculty of Medicine, Charles University, Center for Advanced Preclinical Imaging (CAPI), Salmovská 3, 120 00 Prague, Czech Republic

ARTICLE INFO

Keywords:
mesoporous silica
Gd_2O_3 nanoparticles
drug delivery
MRI
5-Fluorouracil

ABSTRACT

We have prepared silica matrix with hexagonal symmetry of pores (SBA-15) and loaded it with anticancer drug 5-Fluorouracil (5-FU) to promote it as a drug delivery system. Gd_2O_3 nanoparticles were incorporated into the matrix to enhance nanosystems applicability as contrast agent for MRI, thus enabled this nanocomposite to be used as multifunctional nano-based therapeutic agent. Drug release profile was obtained by UV-VIS spectroscopy, and it indicates the prolongated release of 5-FU during the first hours and the total release after 5 h. The cytotoxicity tests using MTT-assay, fluorescent microscopy, bright-field microscopy, and flow cytometry were carried out using human glioma U87 MG cells and SK BR 3 cells. The nanocomposite with anticancer drug (Gd_2O_3/SBA-15/5FU) showed toxic behaviour towards studied cells, unlike nanocomposite without drug (Gd_2O_3/SBA-15) that was non-toxic. Our drug delivery system was designed to minimalize negative effect of Gd^{3+} ions at magnetic resonance imaging and drug 5-FU on healthy cells due to their encapsulation into biocompatible silica matrix, so the Gd^{3+} ions are more stable (in comparison to chelates), lower therapeutic dose of 5-FU is needed and its prolongated release from silica pores was confirmed. Very good T1 contrast in MR images was observed even at low concentrations, thus this nanosystem can be potentially used as contrast imaging agent.

1. Introduction

Through the years of development, many new drugs were discovered by the employment of combinatorial screening, but ca. 40 % of newly discovered drugs suffers from low absorption and bad bioavailability [1]. However, many of these drugs show good effectivity in in-vitro studies. To overcome the hydrophobic nature of some drugs, researchers developed various types of drug delivery systems,

* Corresponding author
E-mail address: adriana.zelenakova@upjs.sk (A. Zeleňáková).

https://doi.org/10.1016/j.heliyon.2023.e20975
Received 9 June 2023; Received in revised form 28 September 2023; Accepted 12 October 2023
Available online 14 October 2023

such as liposomes [2], beads [3] and nanoparticles [4–7]. Apart from traditional chemical synthesis, nanoparticles can even be prepared using parts of plants [8].

In recent years, the use of nanoparticles in medicine has received a lot of attention. Many nanomaterials find their application in diagnostics as well as in therapy [9]. Mesoporous silica is one of the promising nanomaterials which can carry the molecules of drug and according to surface modification, can overcome many problems linked to drug delivery [10,11]. Mesoporous silica as a drug delivery system can significantly improve the solubility of the hydrophobic drug [12], release it at a prolonged time [13], or isolate molecules of the drug to the time when they reach the target tissue [14].

Nanomaterials also can be used as contrast agents in magnetic resonance imaging [15]. In 1988 gadolinium-based MRI (Magnetic Resonance Imaging) contrast agents were first approved for clinical use [16]. Gadolinium (Gd) belongs to the group of lanthanides. It has high paramagnetic properties and strong relaxation effect owing to seven unpaired electrons in the 4f shell [17]. Gadolinium is such a unique element that can be also applied in the form of its oxide as a contrast agent [18]. Furthermore, gadolinium oxide can be used simultaneously in X-ray tomography, neutron capture therapy and magnetic resonance imaging [19]. Nowadays, gadolinium-based contrast agents (GBCAs) in which Gd^{3+} occurs in chelated form belongs to the most widely used contrast mediums, but Gd^{3+} ions can break free from the Gd/chelate compound and thus have toxic side effects. Due to this disadvantage, there is an effort to develop other methods to stabilize Gd^{3+} ions, so they can be used in contrast mediums [20].

One of the potential solutions is preparing Gd nanoparticles and integrating them into biocompatible silica matrix. In this aspect, mesoporous silica (MPS) has also a great potential as drug delivery system. Typical MPS has a large specific surface area to weight ratio and ability to modify the surface by various organic groups, and thereby affect the interactions between surface and biologically active molecules [21]. Such nanocomposite systems exhibit promising properties regarding efficient drug delivery or tracking and targeting their movement in the living organism. We have prepared mesoporous silica matrix with incorporated Gd_2O_3 nanoparticles as a drug delivery system (DDS) for anticancer drug 5-Fluorouracil (5-FU). The presented DDS was also investigated as a contrasting agent that can be utilised to monitor the position of the drug in the body by MRI (Fig. 1).

For the DDS of drug 5-FU also similar system was prepared, by Xiaoxiao Sun et al. [22], who prepared pH-sensitive ZnO/-carboxymethyl cellulose/chitosan bio-nanocomposite beads for controlled release of 5-FU. They have observed, that within first 2 h, lower amount of 5-FU (<20 %) was released from ZnO/CMC/CS beads at low pH = 1.2) and in pH = 6.8 overall cumulative release reached 80 % after 5 h. The increase of pH enabled more water molecules inside the ZnO/CMC/CS beads, making it easier for 5-FU to release [22].

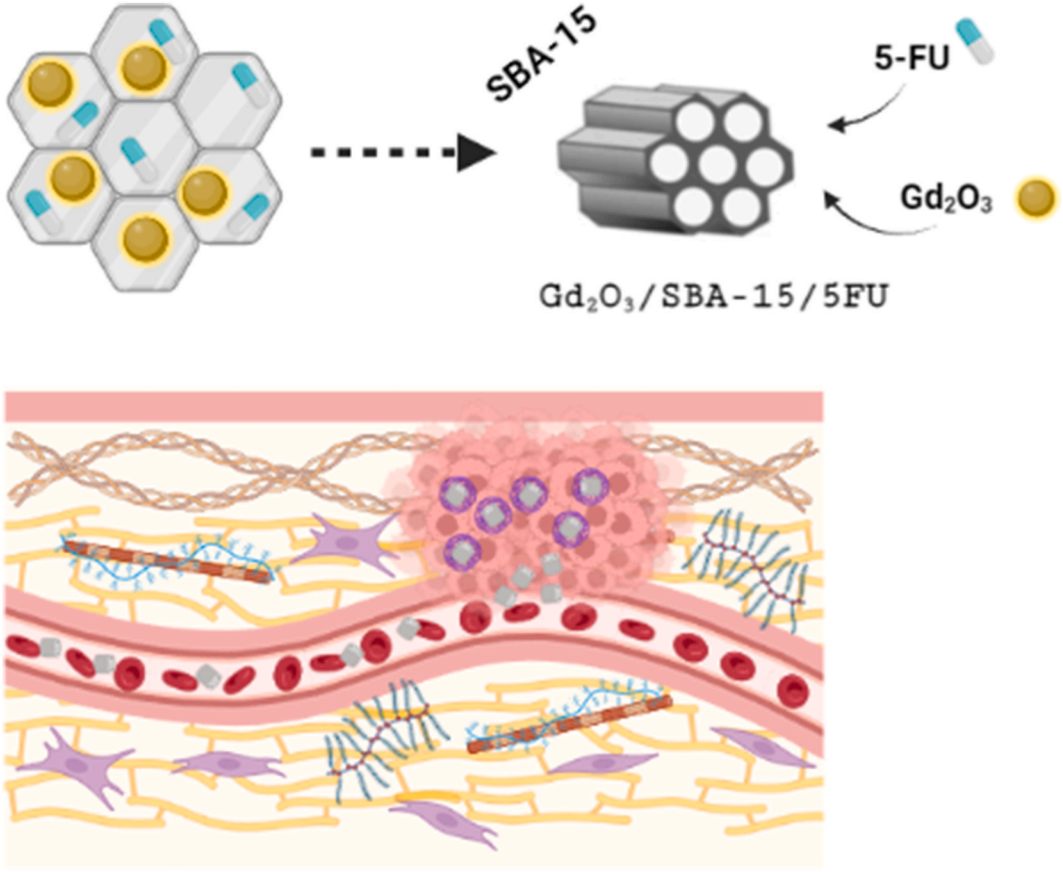

Fig. 1. Scheme of Gd_2O_3/SBA-15/5FU nanocomposite and its application (created with BioRender.com).

2. Experimental

2.1. Materials

All of the chemicals: 99.9 %, $Gd(NO_3)_3 \times 6H_2O$, 98 % TEOS – tetraetoxysilane, 35 % HCl, 5-Fluorouracil (5-FU), Pluronic P-123, Pluronic F-127 were obtained from Sigma-Aldrich. The chemicals were utilised without any further purifications. In all of the performed experiments, deionised water was employed.

2.2. Synthesis of nanocomposite Gd_2O_3/SBA-15/5FU

We have prepared Gd_2O_3/SBA-15 nanomaterial using the nanocasting method. Foremost, 1 g of dry SBA-15 (Santa Barbara Amorphous-15), which was prepared according to Ref. [16], was impregnated with $Gd(NO_3)_3$ (Sigma-Aldrich) (0.5 M solution, 20 ml) for 2 h at laboratory temperature. After impregnation the product was filtered and allowed to dry for 2 h at 323 K. Afterwards, prepared Gd_2O_3/SBA-15 was calcined for 3 h at rate 1 K/min up to 773 K. The 5-Fluorouracil (5-FU) (Sigma-Aldrich) was loaded into the Gd_2O_3/SBA-15 by incipient wetness impregnation method. First, the saturated solution (10 mg/ml) of 5-FU in water at room temperature was prepared. In the next step, 1 g of mesoporous silica modified with Gd_2O_3 nanoparticles was impregnated with 5-FU solution. The capillary action drew the solution into the pores till incipient wetness. The product of the impregnation was dried, and the process was repeated twice. The amount of the drug loaded in the pores was determined by elemental analysis (see paragraph 3.4). The final prepared nanocomposite was denoted as Gd_2O_3/SBA-15/5FU.

2.3. Zeta potential and hydrodynamic size measurement

Measurement of Zeta potential (ZP) and hydrodynamic size of nanoparticles was realized on ZetaSizer Nano ZS (Malvern Panalytical) at temperature 25 °C and at different values of pH including pH = 7.4 and 2. Both parameters were measured using the DLS (Dynamic Light Scattering) method and the samples were analysed in form of dilute suspension of particles in an aqueous solution. Samples were sonicated for 10 min before measurement. Each value of ZP was calculated using Smoluchowski approximation and was obtained as standard statistical value from 30 points.

2.4. Magnetic measurements

Measurements in applied DC and AC magnetic field up to 5 T were carried out in temperature range 2–325 K by using SQUID-based magnetometer MPMS 5XL (Quantum Design, Inc.). The powder sample was secured against movement and placed into the plastic holder. The same sample setup was used for differential AC susceptibility measurements in external applied magnetic fields of 1000, 2000 and 3000 Oe and temperatures 4.5 K and 8 K.

2.5. Drug release

Sample with encapsulated drug 5-FU (10 mg) was placed in a plastic vial and mixed with saline solution with pH = 7.4. The mixture was gently stirred using rotator. The solution was analysed in different time intervals: 1, 2, 3, 5 and 24 h. The total amount of released drug was determined using UV-VIS (Ultraviolet–Visible) spectroscopy at 266 nm. Calibration curve was constructed using 5-FU standard. The correlation coefficient was $r^2 = 0.99996$.

2.6. Cell culture

The SK BR 3 (human breast adenocarcinoma, a gift from prof. Pluckthun laboratory, University of Zurich, Switzerland) as well as U87 MG (human glioma purchased from Cells Lines Services, Germany) were grown in culture media (Dulbecco's modified Eagle medium, D-MEM, Gibco-Invitrogen, Life Technologies Ltd., and RPMI 1640, LM-R1638/500, biosera) supplemented with sodium pyruvate (110 mg/l), L-glutamine (862 mg/l), glucose (4500 mg/l), 10% fetal bovine serum (FBS) and penicillin/streptomycin (1% w/w) in the dark at 37 °C, 5% CO_2 under humidified atmosphere until 80% confluence (solutions were obtained from Gibco-Invitrogen, Life Technologies Ltd.).

2.7. MTT-assay

The MTT assay is used to measure cellular metabolic activity as an indicator of cell viability, proliferation and cytotoxicity. This colorimetric assay is based on the reduction of a yellow tetrazolium salt (3-(4,5-dimethylthiazol-2-yl)-2,5-diphenyltetrazolium bromide or MTT) to purple formazan crystals by metabolically active cells. U87 MG cells were incubated for 24, 48 and 72 h in the absence and presence of distilled water (10, 50 and 100 μl/ml), Gd1 and Gd2 in complete cell culture media. The examination of cell viability was performed by MTT (3-(4,5-dimethylthiazol-2-yl)-2,5-diphenyltetrazolium bromide, Sigma-Aldrich, Germany) assay detected at 560 nm and 750 nm by 96 well plate absorption reader (GloMax®-Multi + Detection System with Instinct Software, Promega Corporation, USA). The MTT assay was evaluated by standard protocol: Phosphate saline buffer (PBS, pH = 7.4) was used to dissolve 10 μl of 5 mg/ml MTT that were added into each well containing 100 μl medium (alternatively, Petri dish was employed to accommodate

100 μl of MTT added into 1 ml media) and during 1 h the plate was incubated at 37 °C in the dark; after 1 h the cell culture medium was removed from the well and 200 μl (alternatively 1 ml in Petri dish) of dimethylsulfoxide (DMSO, Sigma-Aldrich, Germany) were added into each well to dissolved formazan crystals. Microscopical images of U87 MG cells with formazan crystals were detected prior to DMSO addition. The standard derivation (SD) from the mean values of experimental data (performed in triplicates) is represented by errors. The T-test were utilised to estimate the level of significance: *$p < 0.05$, **$p < 0.01$, ***$p < 0.001$.

2.8. Fluorescence microscopy

The glass coverslip bottom Petri dishes (35 mm, No. 0, MatTek, USA) were used for cells growth at the density 105 cells. Bright field images of cells in the presence of Gd1 and Gd2 nanoparticles were detected before (at concentrations 10 μl/ml) and after nanoparticles filtration via 0.22 μm filter (at concentrations 100 μl/ml). SK BR 3 cells were detected in the presence of 30 μl/ml nonfiltered nanoparticles. Cell culture media with nanoparticles were maintained during imaging. Cell culture media were removed and replaced by fresh one prior fluorescence staining. Mitochondria were stained with MitoTracker® Orange CMTM/Ros (MTO, 0.2 μM, 15 min, ThermoFisher Scientific, USA). 10 μg/ml Hoechst 33258 (Hoechst, 15 min, ThermoFisher Scientific, Slovakia) was used to stain cell nuclei with and phosphatidylserine was labeled with AnnexinV/FITC (5 μl from the detection Kit, 15 min, Annexin V-FITC Kit, Miltenyi Biotec, Germany). To visualize the cells an inverted LSM700 confocal microscope (Zeiss, Germany) was employed, with a CCD camera (AxioCam HRm, Zeiss, Germany) and a 20X Fluar (NA = 0.75, ∞, Zeiss, Germany). The excitation of MTO fluorescence was carried out by 555 nm cw solid-state laser, while the detection of emission was performed >580 nm. The 405 nm laser was employed for Hoechst excitation (emission detected in the range 410–490 nm). AnnexinV/FITC was excited at 488 nm and detected in the range 500–540 nm. The Zen 2011 software (Zeiss, Germany) or ImageJ software (National Institutes of Health, USA) were utilised for the fluorescence analysis. The same microscope was employed for the bright-field images acquisition.

2.9. Flow-cytometry

Petri dish (round, 35 mm, 80% confluence) was utilised for SK BR 3 growth. The cells were subjected for 48 h to 30 μl/ml to Gd1 and Gd2 nanoparticles in complete cell culture medium and subsequently analysed. Before the flow-cytometric measurement, cell pellet, harvested by Trypsin-EDTA (ThermoFisher Scientific, USA) and centrifuged (1000 rpm/8 min) was resuspended in PBS (500 μl, contained 50 μl of 10x Annexin V binding buffer). Side scatter (SSC) values keep the information about internal complexity of the cells. Forward scatter (FSC) values determine cell populations according to their size. FSC, SSC, MTO and FITC fluorescence values were estimated by flow-cytometry (MACSQuant® Analyzer, Miltenyi, Germany). Apoptotic cell populations were defined with Annexin V/FITC (B1 channel, ex-citation $\lambda_{exc} = 488$ nm and emission $\lambda_{em} = 525 \pm 50$ nm) staining according to the protocol. Overall, 10 000 cells were divided into four quadrants according to Annexin V/FITC and MTO (B2 channel, excitation $\lambda_{exc} = 488$ nm and emission $\lambda_{em} > 585 \pm 40$ nm) staining. Right side quadrants indicate apoptotic cells.

2.10. MR imaging

To demonstrate a potential ability to track the nanoparticles using MRI, a phantom containing nanoparticle suspensions was prepared and scanned in an experimental 1 T MRI scanner ICON (Bruker BioSpin; Ettlingen, Germany). Nanoparticles at clinically relevant concentrations (0, 1, 2, 5, 10 mM Gd) were dispersed in 4% porcine gelatine (Sigma-Aldrich, St. Louis, MO, USA) to avoid flow/diffusion or sedimentation during the scanning, and biologically stabilized by 0.2% sodium azide. The volume of each sample was 200 μL. A T1-weighted spin echo sequence (echo time TE = 3.51 ms, TR = 240 ms) and a T2-weakly weighted turbospin echo sequence (effective TE = 10.54 ms, TR = 4000 ms) were used with the same geometry (2 mm horizontal slices, 16 × 32 mm^2 field of view, 64 × 128 matrix).

2.11. NMR relaxometry

To evaluate the suitability of the present Gd_2O_3/SBA-15 sample as contrast agents for MRI, a ^{1}H NMR (Nuclear Magnetic Resonance) relaxometry study was carried out on aqueous suspensions of the powder sample in the magnetic field of magnitude 0.47 T (^{1}H Larmor frequency of 20 MHz). The molar concentration of Gd in the suspension was 73 mmol L^{-1}, and the resulting suspensions were measured at 23 and 37 °C with a MiniSpec mq20 relaxometer (Bruker BioSpin; Ettlingen, Germany). T1 (longitudinal relaxation times), were determined by a saturation-recovery pulse sequence (10 points with varying recovery times in the range of 5–500 ms at 23 °C and 3–300 ms at 37 °C). Five values of T1 were obtained for each temperature and their average is presented. Samples were vortexed between each run to prevent sedimentation of suspension. Relaxivities r1 were calculated as a ratio of average relaxation rate R1 (reciprocal values of T1) at given temperature and molar concentration of Gd. Relaxivity at the magnetic field of 11.7 T was measured on Bruker Avance III spectrometer with ^{1}H Larmor frequency of 500 MHz equipped with BBFO probe. Three samples of aqueous suspension of Gd/SBA-15 with the concentration of 73, 36.5 and 18.3 mmol L^{-1} were prepared in 5 mm NMR tubes and the resulting suspensions were measured at 23 °C. T1 (longitudinal relaxation times) were determined by inversion-recovery pulse sequence (10 points with varying recovery times in the range of 5–500 ms). Three values of T1 were obtained for each concentration and their average is presented. Samples were vortexed between each run to prevent sedimentation of suspension. Relaxivities r1 were calculated by using a linear fit of the dependence of relaxation rates R1 (reciprocal values of T1), on the molar concentration of Gd in Gd_2O_3/SBA-15 suspension.

3. Results and discussion

3.1. Physicochemical and structure characterization

Transmission electron microscopy (TEM) images shown in Fig. 2 obtained by JEOL 2100 microscope (Jeol, Ltd.) described the structure of silicon matrix and the hexagonal symmetry of pores, as it is typical for SBA-15. Pores are approximately 7 nm wide and inside the pores the gadolinium oxide nanoparticles and drug 5-FU are incorporated. On the left side of Fig. 2, the blank silica is pictured in longitudinal direction (Fig. 2 A) to pore axis and in transversal direction (Fig. 2 B). On the right side the pores filled with nanoparticles can be seen (Fig. 2C and D). The energy dispersive X-Ray analysis (EDX, Fig. 2 bottom) has confirmed the presence and uniform distribution of Gd_2O_3 particles inside the silica pores. From EDX analysis the atomic percentual content of O_2 (blue) was 37.75 %, content of Si (yellow) was 22.75 % and Gd (red) was presented in 39.5% of total volume of the sample. The confirmation of presence of Gd_2O_3 nanoparticles inside porous matrix, the morphology and the phase composition were investigated by the XANES (X-ray Absorption Near Edge Structure) measured at synchrotron, and the results were presented in our earlier studies [23–25]. We also conducted the SANS (Small Angle Neutron Scattering), XPS (X-Ray Photoelectron Spectroscopy), HE-XRD (High-Energy X-Ray Diffraction), measurement that confirmed the spherical shape of nanoparticles and their presence inside silica pores. XANES spectra of studied sample Gd_2O_3/SBA-15 and reference foil Gd_2O_3 confirm the presence of pure Gd_2O_3 nanoparticles incorporated in porous matrix. The results of the XPS analysis evidenced the chemical composition of examined Gd_2O_3/SBA-15 sample without contamination by other compounds. This presence of only Si, Gd, and O atoms has been confirmed in the studied sample. The XPS analysis clearly revealed essentially broader Gd 4*d* peaks in core-level spectra. The valence band (VB) area up to 30 eV was recorded for the samples and compared with that of the Gd-O_x XPS external standard [23].

The IR (Infra-Red) spectroscopy evidenced the presence of 5-FU in the silica matrix pores. Also, nitrogen sorption analysis of the sample, presented in our previous work [24], confirmed the reduction of free space inside silica pores after incorporating Gd_2O_3 nanoparticles. The behaviour of adsorption isotherms proved the decrease of free space (S_{BET}) with increasing concentration of nanoparticles in the sample, where the value of S_{BET} for blank SBA-15 was 708 $cm^2\ g^{-1}$ and dropped to 100.53 $cm^2\ g^{-1}$ after Gd_2O_3 incorporation [24].

3.2. Determination of hydrodynamic size and Zeta potential

The hydrodynamic particle size and Zeta potential (ZP) were measured to determine the biocompatibility, colloidal stability and nanosystems suitability for the application into living organisms. At pH = 7, the value of hydrodynamic size for the sample without 5-FU was 308 d nm and for the sample with loaded drug about 350 d nm. The hydrodynamic size was relatively preserved after the 5-FU was incorporated into the pores. The very high value of hydrodynamic size at pH = 2 indicated aggregation of nanoparticles due to strong dipolar interactions. For comparison, the ZP was also measured for the pure SBA-15 matrix, which at pH = 7 showed an optimal ZP value (−33.8 mV). The sample with incorporated nanoparticles already showed increased negative values of ZP and after the addition of the drug the value increased up to −85 mV, which could be caused by the modification of the surface charge by a non-polar agent that contained the drug. With increasing value of pH and progressive dissociation of Si–OH groups on the surface the ZP becomes more negative. The values of hydrodynamic size can be seen in Fig. 3 and values of ZP in Fig. 4.

3.3. Magnetic properties of Gd_2O_3/SBA-15/5FU

Magnetic properties were measured in applied external DC field up to 5 T at three temperatures: 2, 100 and 300 K (Fig. 5 – insert). The curves showed the typical paramagnetic behavior at temperatures 100 K and 300 K, due to the presence of Gd^{3+} ions. The configuration of Gd^{3+} is [Xe]6*s*25*d*14*f*7 means that there are 7 unpaired electrons in the 4*f* shell. They polarize the valence electrons (6*s* and 5*d*) what results in a calculated magnetic moment of 7.88 μ_B/Gd^{3+}. These localized magnetic spins of Gd^{3+} induce only paramagnetic moment [26,27]. Similarly, as in our system, the paramagnetism was observed at room temperature in pure Gd_2O_3 nanoparticles as well as in Gd-doped oxide semiconductors [26]. At the temperature 2 K the magnetization curve (magenta) attempts to accommodate the shape of hysteresis and reaches very high magnetization.

The zero-field cooling (ZFC) and field cooling (FC) magnetization curves are completely overlapped in temperature range 2–300 K and the curves exhibit the Curie–Weiss behavior characteristic of paramagnetism, see Fig. 5. The temperature dependence of inverse magnetic susceptibility, calculated from FC magnetization, perfectly follows the Curie–Weiss law and a linear fit gives values of $\Theta = -2.04$ K. The negative sign of Curie–Weiss temperature is indicative of the presence of antiferromagnetic exchange interaction between Gd^{3+} ions. The origin of antiferromagnetic interaction at very low temperature is due to the suppression of thermal randomization of fluctuating magnetic spins of Gd^{3+} ions. It is necessary to note, that the magnetic behavior of studied nano-cargo system of Gd_2O_3/SBA-15/5FU is completely caused by behavior of Gd_2O_3 nanoparticles without any magnetic influence of diamagnetic silica SBA-15 or drug 5-FU. The magnetism of pure mesoporous silica was previously studied in our earlier work [28].

On the Gd_2O_3/SBA-15 sample the dependencies of the real and imaginary components of the differential AC susceptibility on the frequency in the fields 1000, 2000 and 3000 Oe and at temperatures of 4.5 K and 8 K were measured, as can be seen in Fig. 6 (A, B, C). Measurements of AC susceptibility showed that there is a magnetic interaction in the systems, which can be identified from the values of maxima at χ''. The long-range antiferromagnetic interaction between Gd^{3+} ions at very low temperatures was confirmed, which was also confirmed from measurements in the DC field.

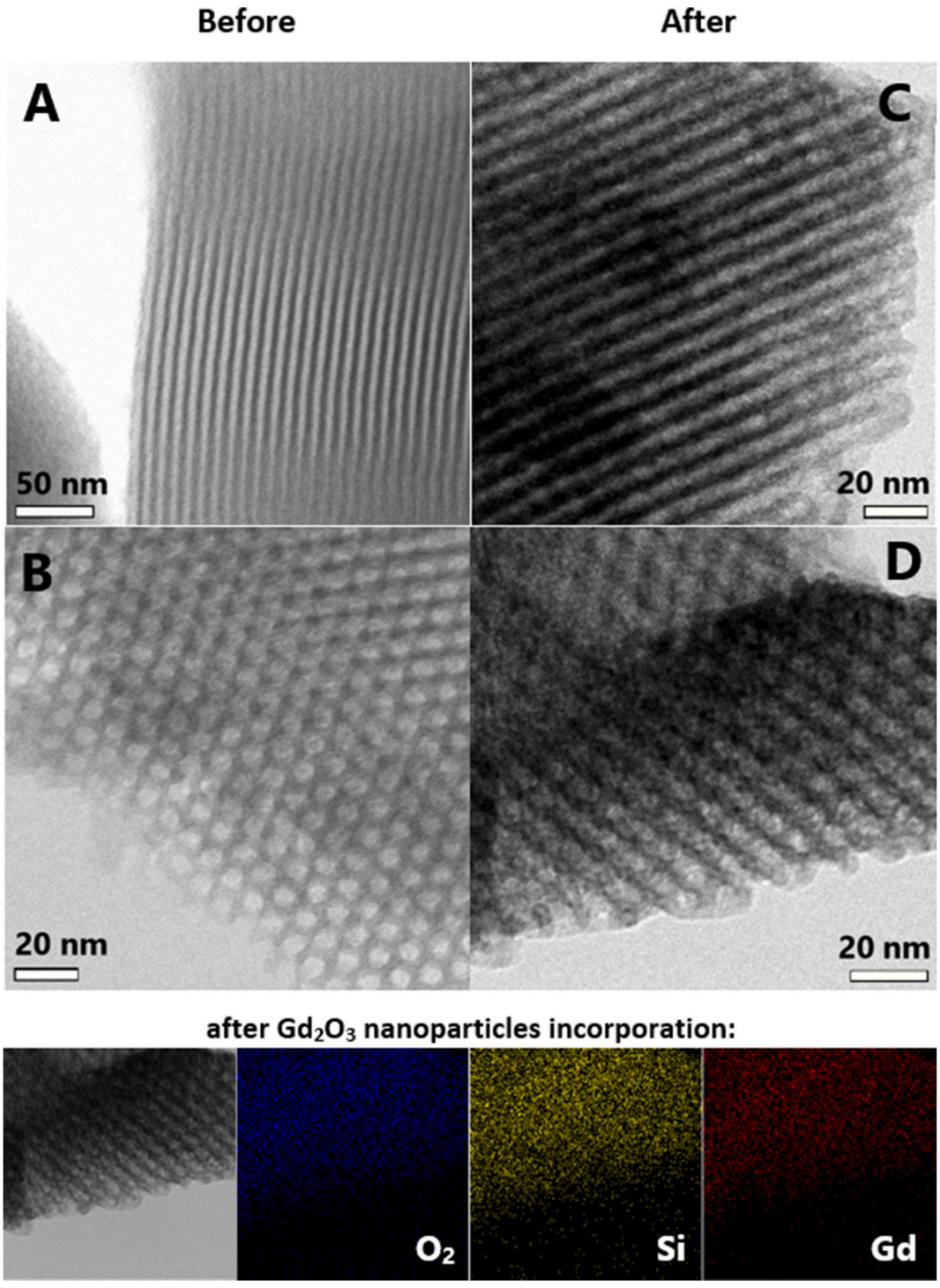

Fig. 2. TEM images of sample Gd_2O_3/SBA-15: A, B represents blank silica; C, D represents the silica after incorporation of Gd_2O_3 nanoparticles. At the bottom, the EDX analysis after Gd_2O_3 incorporation is presented.

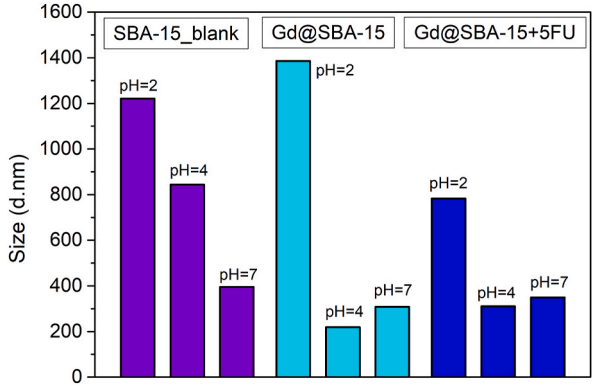

Fig. 3. Size distribution of samples SBA-15 (blank), Gd@SBA-15 (Gd_2O_3/SBA-15) and Gd@SBA-15+FU (Gd_2O_3/SBA-15/5FU) at pH = 2, 4, 7.

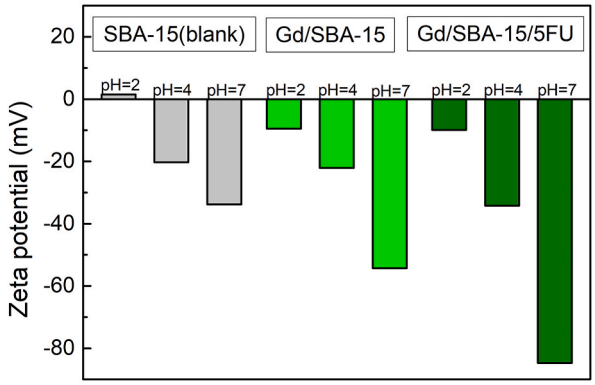

Fig. 4. Zeta potential of samples SBA-15 (blank), Gd@SBA-15 (Gd_2O_3/SBA-15) and Gd@SBA-15+FU (Gd_2O_3/SBA-15/5FU) at pH = 2, 4, 7.

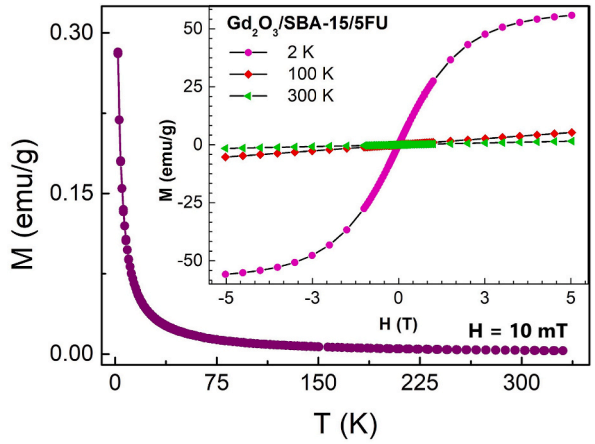

Fig. 5. Magnetization dependence on temperature (ZFC-FC mode) and on external applied magnetic field (insert) at temperature 2, 100 and 300 K.

3.4. Drug release experiment

A drug release study was performed in physiological solution at pH 7.4. By elemental analysis we have determined the total amount of drug (5-FU) inside the silica pores. From synthesis point of view, 100 mg of nanoparticles was immersed in 10 ml of 10 mg/ml solution of 5-FU. The total loaded amount of 5-FU from UV-VIS spectroscopy was established to be 580 mg of 5-FU per 1 g of solid Gd_2O_3/SBA-15/5FU. The amount 580 mg/g was taken as 100 % in the release study and was used to calculate the percentage of the released amount in the respective time intervals. The experimental results are given in Fig. 7. It is evident that drug release occurred

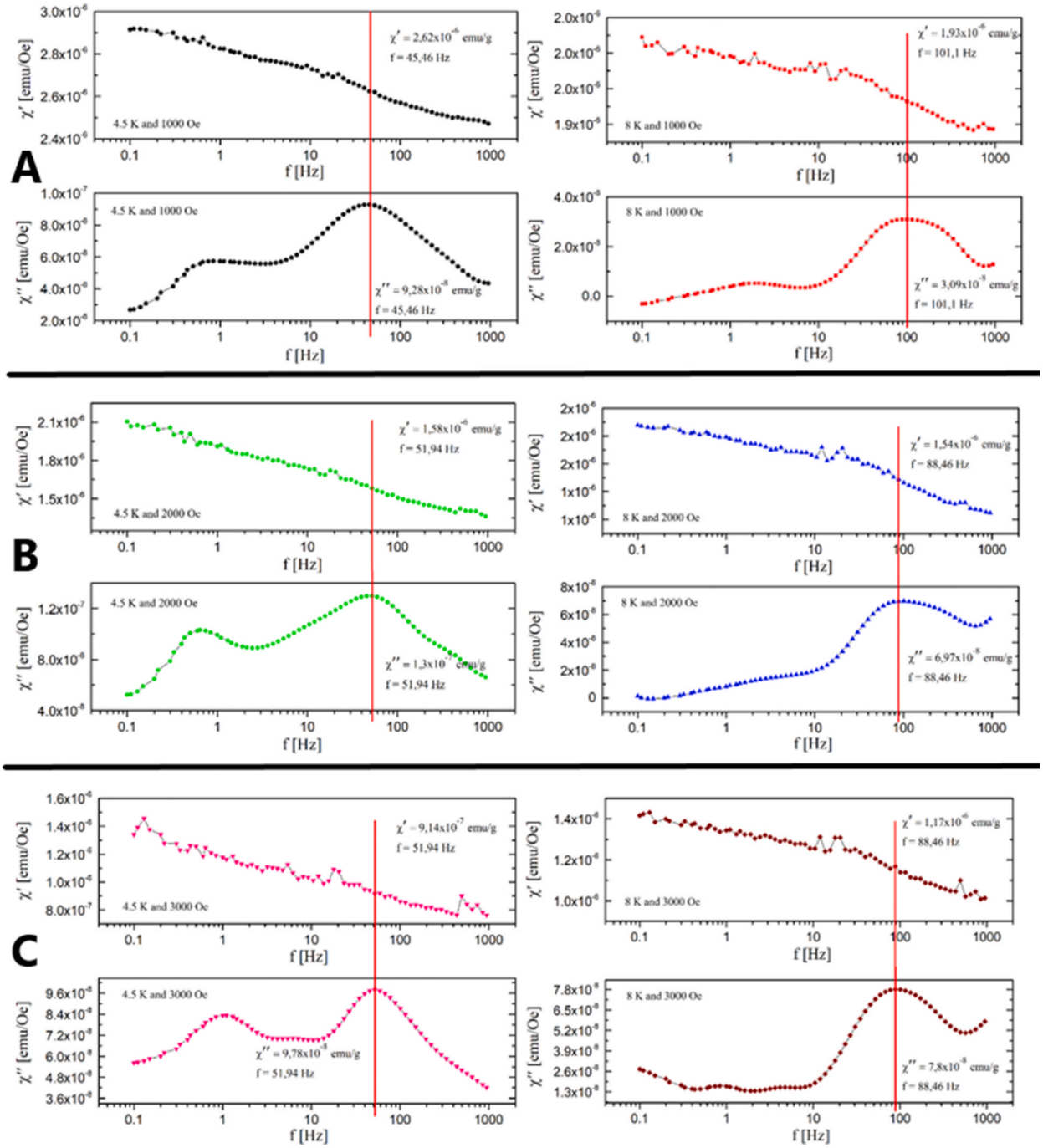

Fig. 6. Real and imaginary component of AC susceptibility of Gd_2O_3/SBA-15 sample in magnetic field 1000 Oe (A), 2000 Oe (B) and 3000 Oe (C), and temperatures 4.5 K (left) and 8 K (right).

rapidly during the first hours of release and the total release occurred after 5 h. Such a rapid and sudden release of drug is commonly observed in mesoporous matrices with open porous structure. Moreover, the 5-fluorouracil is a small molecule with molar weight of 130.1 g/mol with no strong interactions with silica surface. Also, in Fig. 7 the calibration curve with deviation below the resolution value of the measuring device is included (Fig. 7 – insert). Therefore, we assumed a 2% measurement deviation.

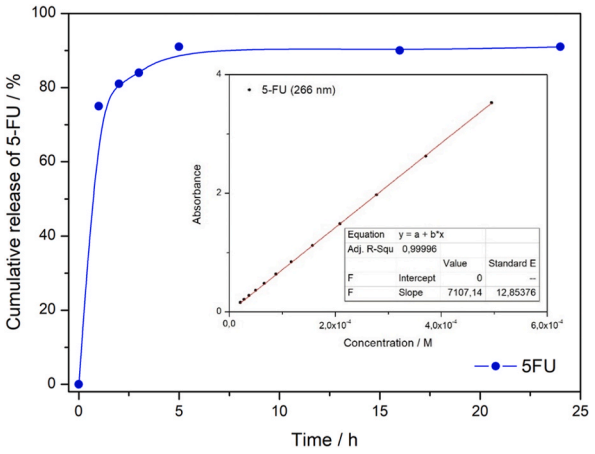

Fig. 7. Cumulative release of 5-FU from Gd_2O_3/SBA-15/5FU (insert: calibration curve of 5-FU at $\lambda = 266$ nm).

3.5. *In-vitro cytotoxicity*

In the following cytotoxicity study, the samples were denoted as follows: Gd_2O_3/SBA-15 as Gd1 and Gd_2O_3/SBA-15/5FU as Gd2. Representative images of formazan production in U87 MG cells in the absence and presence of 100 μl/ml Gd1 (Gd_2O_3/SBA-15) and Gd2 (Gd_2O_3/SBA-15/5FU) nanoparticles detected 24 h after their administration can be seen in Fig. 8 A. The cytotoxic effect of Gd2 was examined on U87 MG cells utilizing MTT test (colorimetric assay) (Fig. 8 B), distribution of Gd1 and Gd2 in U87 MG cells (Figs. 9 and 10) and dissipation of $\Delta\Psi_m$ and apoptotic features in U87 MG cells in the presence of Gd1 and Gd2 nanoparticles (Figs. 11 and 12).

MTT-assay was performed 24, 48 and 72 h after nanoparticles administration, and it it pictured on Fig. 8 below. Production of formazan in U87 MG cells incubated with Gd1 was minimally affected (only 20% decrease), but the significance of its influence increased with time (72 h) and concentration (100 μl/ml). In contrary, application of Gd2 nanoparticles resulted in significant decrease in formazan production (below 40% at 100 μl/ml at 72 h incubation). Low effectivity of formazan production can be seen in bright-field image of U87 MG cells incubated with Gd2 nanoparticles. Bright-field images of U87 MG cells (Fig. 9) in the presence of Gd1 (Fig. 9 A, B) and Gd2 nanoparticles (Fig. 9C, D) were detected 24 h after nanoparticles administration. Extracellular area with nanoparticles and aggregates of nanoparticles is zoomed in the inserts.

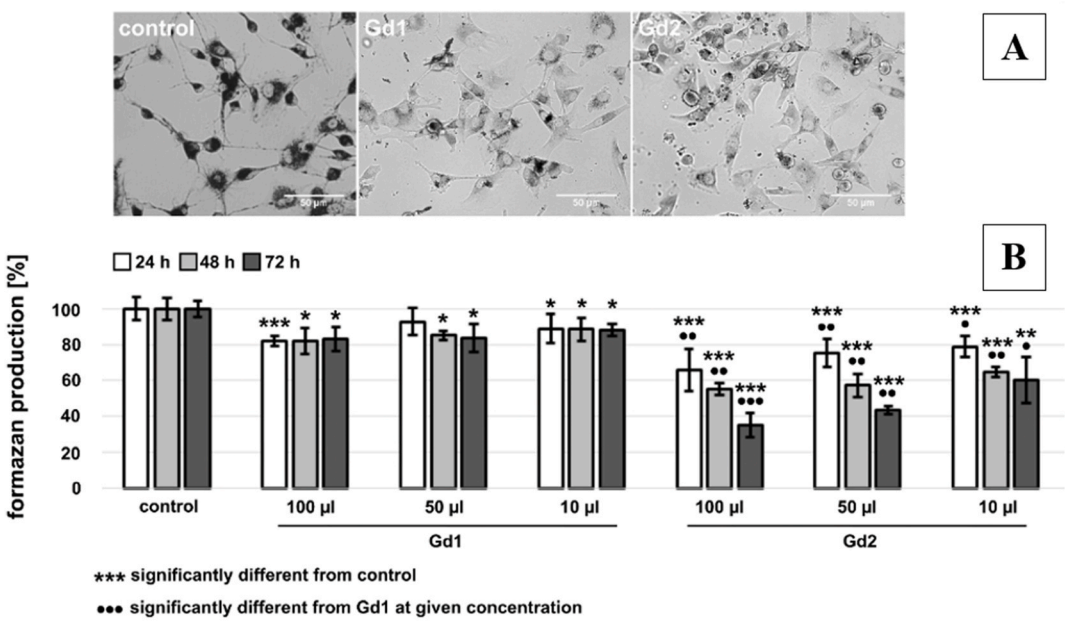

Fig. 8. A. Representative images of formazan production in U87 MG cells in the absence and presence of 100 μl/ml Gd1 (Gd_2O_3/SBA-15) and Gd2 (Gd_2O_3/SBA-15/5FU) nanoparticles detected 24 h after their administration. B. Production of formazan (related to the viability of cells) in U87 MG cells in the absence and presence of 10, 50 and 100 μl/ml of Gd1 and Gd2 nanoparticles.

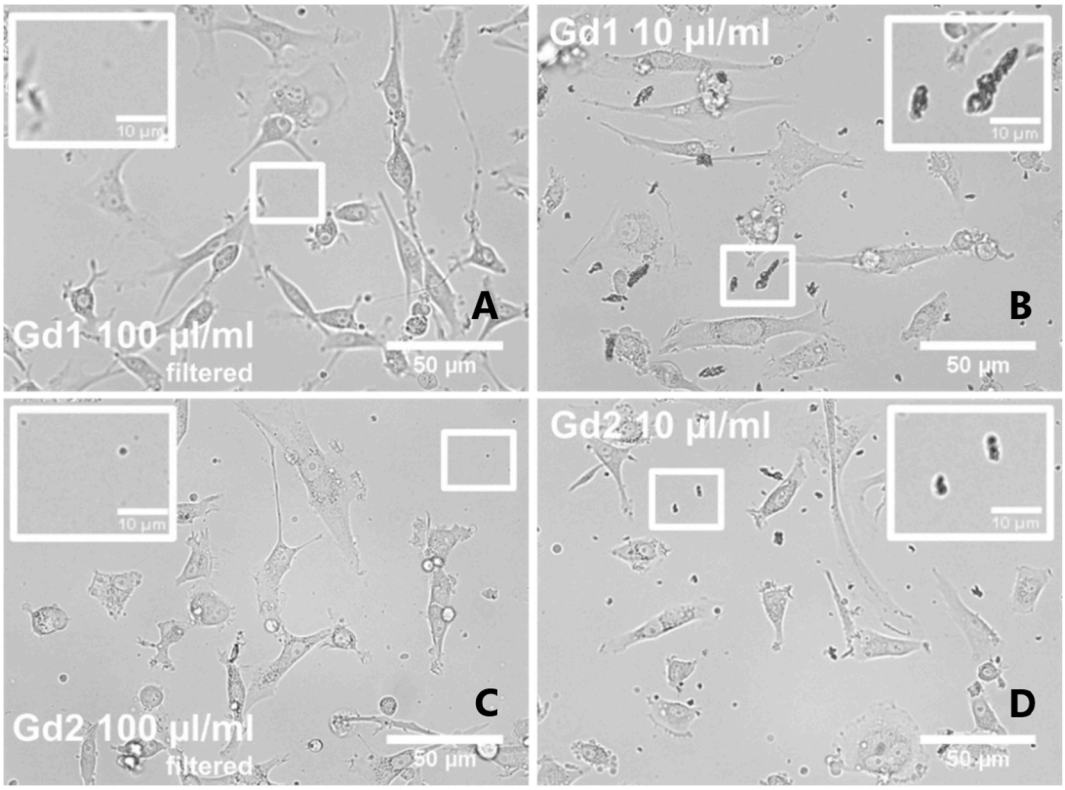

Fig. 9. Bright-field images of U87 MG cells in the presence of Gd1 (Gd_2O_3/SBA-15) (A, B) and Gd2 (Gd_2O_3/SBA-15/5FU) (C, D) nanoparticles before (10 µl/ml) and after nanoparticles filtration (100 µl/ml). The control group is similar to Figs. 10 and 11.

The morphology of U87 MG cells has been revealed by Bright-field images and it is not significantly changed in the presence of Gd1 nanoparticles. Localisation of nanoparticles (dark spots) within the cells and in the extracellular area is demonstrated in zoomed images (Fig. 10). Large clusters of nanoparticles aggregates were observed in U87 MG cells incubated with non-filtrated nanoparticles solutions (Fig. 9 inserts). Filtration of nanoparticles enabled disaggregation of nanoparticles, which were transported into the cells. Drug 5-FU loaded in Gd2 was released in cells and significantly affected cell morphology (Fig. 9 - Gd2 100 µl/ml) and viability (Fig. 8 - MTT). Granular shape of the cells refers to cell death. Similar observations were detected in SK BR 3 cells (Fig. 10 A, B, C).

Fluorescence microscopy of Annexin V/FITC fluorescence was performed on U87 MG cells, because of better visualization of these cells. Green fluorescence depicts phosphatidylserine labeled with AnnexinV/FITC probe (15 min, 5 µl/ml), while red fluorescence represents mitochondrial probe MitoTracker Orange CMTM/Ros (15 min, 200 nM), and blue fluorescence represents nuclei labeled with Hoechst (15 min, 10 µg/ml). Externalized phosphatidylserine found in some cells is marked by the white arrow. Overlapped images present all three fluorescence markers, as can be seen in Fig. 11.

SK BR 3 are smaller and much more suitable for flow-cytometric measurement. For this reason, flow-cytometry analysis of Annexin V/FITC fluorescence was detected in SK BR 3 cells. Fluorescence images of control U87 MG cells and cells with Gd1 displayed tubular mitochondria (MTO in red), which are concentrated in the perinuclear area. The mitochondria in the presence of Gd2 were fragmented and more stressed than in control cells. Phosphatydilserine represented in green fluorescence was only detected in cells incubated with Gd2 nanoparticles. These findings suggest that Gd2 sample can trigger apoptosis in U87 MG cells. Similar staining was performed in SK BR 3 cells. Flow-cytometry analysis (Fig. 12) demonstrated two populations of cells: P1 (Fig. 12 A) and P2 (Fig. 12 B) that could correspond to two different phenotypes of cells or two different states of cell differentiation or cell cycle, as can be seen in Fig. 12. Dot plot was divided into four quadrants (upper left – live cells, down left – dissipation of mitochondrial membrane potential ($\Delta\Psi_m$) and upper right – apoptotic cells). The histogram in Fig. 12 below demonstrates the number of events detected in each area.

MTO and AnnexinV/FITC were detected in these populations. AnnexinV/FITC fluorescence distributions present apoptotic cells in P1 and P2 of SK BR 3 cells. These two populations reacted to nanoparticles presence in different manner. Apoptosis defined by Annexin V/FITC fluorescence slightly increased in P1 population in SK BR 3 cells incubated with Gd2. The P2 population was positive for apoptosis in all studied cases. However, Annexin V/FITC histograms are represented by two peaks. In cells incubated with Gd2 nanoparticles the dominant peak was right shifted. These suggest apoptosis induction in SK BR 3 cells incubated with G2 nanoparticles. A certain decrease in mitochondrial membrane potential was detected in P1 population that refers to mitochondrial damage in these cells.

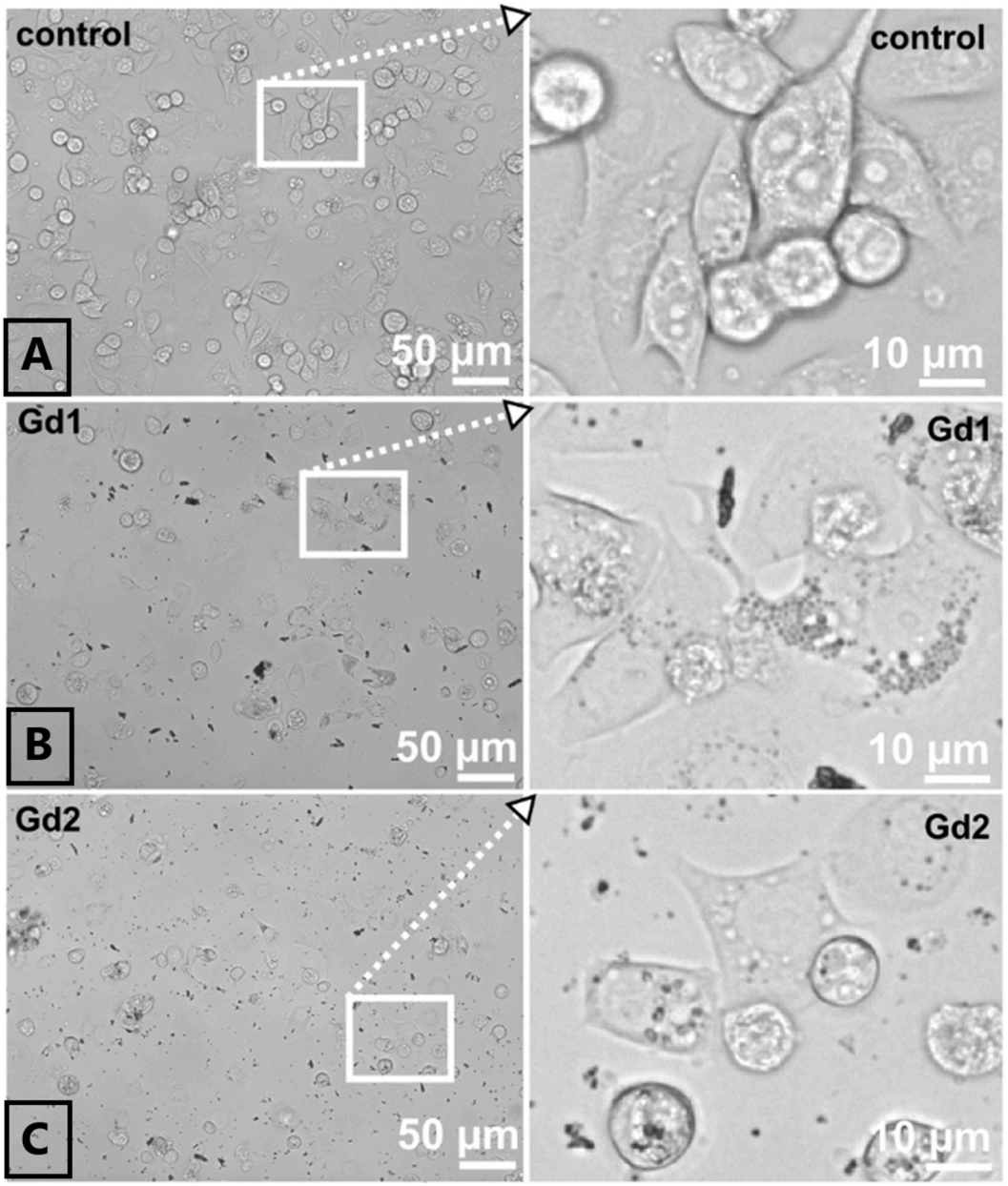

Fig. 10. Bright-field images of SK BR 3 cells in the absence and presence of 30 μl/ml nanoparticles (non-filtered). **A** represents the control, **B** – sample Gd1 (Gd_2O_3/SBA-15) and **C** – sample Gd2 (Gd_2O_3/SBA-15-/5FU). Images were detected 48 h after nanoparticles administration.

MTO is a fluorescent probe that responds to oxidative stress and mitochondrial membrane potential. When mitochondrial membrane potential is depleted, the fluorescence of MTO decreases. For this reason, quadrants were selected to show the cell population with loss of mitochondrial membrane potential in cells. On the other hand, apoptosis-positive cells (AnnexinV/FITC) showed higher MTO fluorescence, which may be attributed to an increase in oxidative stress in the cells due to treatment.

3.6. MR imaging

Nanoparticles can be easily tracked using MRI due to a strong hyperintense signal on T1-weighted images. Strong T1-weighting (Fig. 13a) suppressed the signal from the control sample (a pure gelatin without any nanoparticles), while samples containing nanoparticles provided distinct hyperintense signal. Interestingly, higher concentrations (5, 10 mM) provided lower signal than concentrations 1 or 2 mM due to a signal decrease caused by a T2 effect (the nanoparticles substantially shorten both T1 and T2

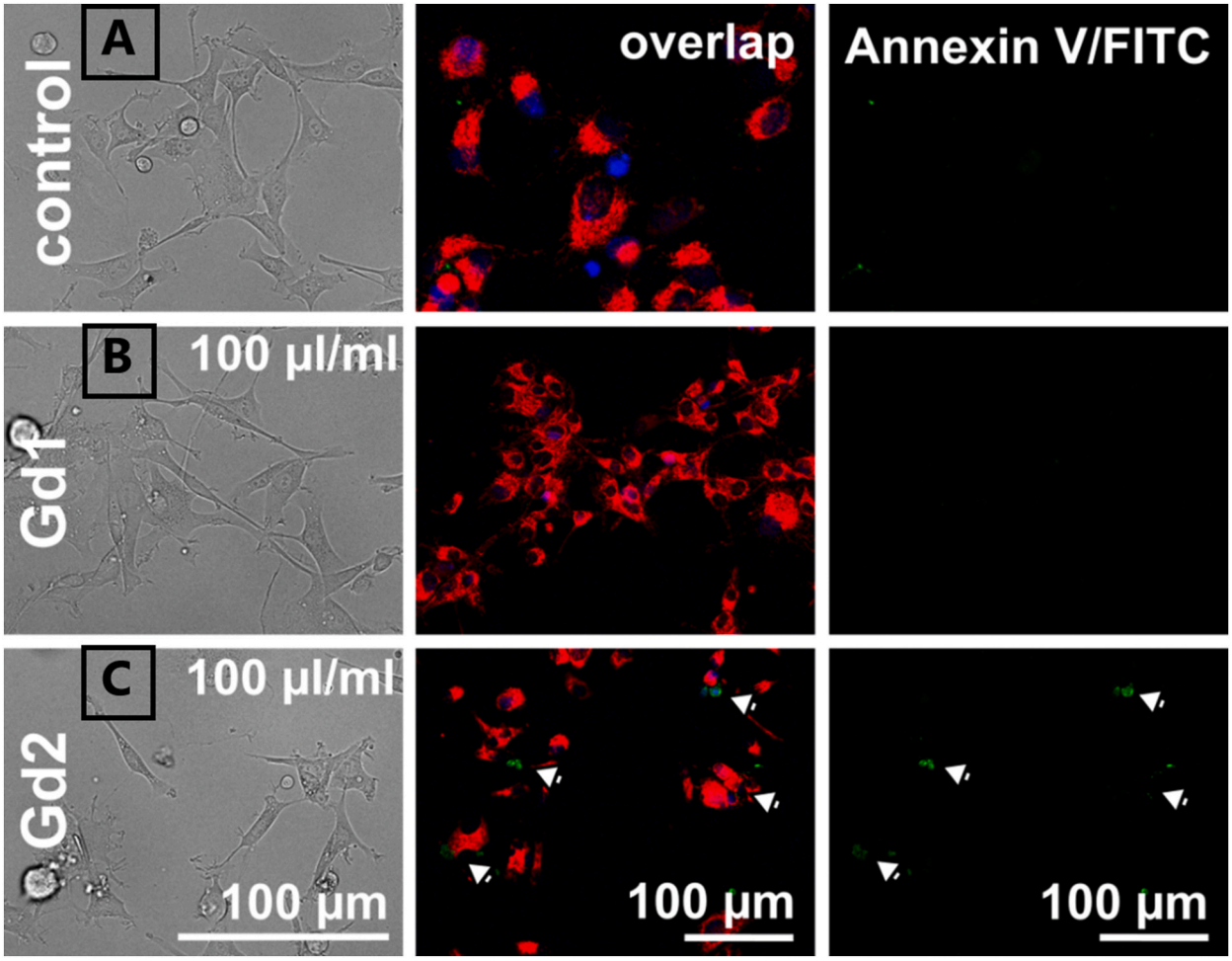

Fig. 11. Bright field and fluorescence images of U87 MG cells in the presence of 100 µl/ml of nanoparticles. **A** represents the control group, **B** – sample Gd1 (Gd_2O_3/SBA-15) and **C** – sample Gd2 (Gd_2O_3/SBA-15/5FU).

relaxation times). This is documented in Fig. 13b, which presents a T2-weighted image. Although T2-weighting was very weak (TE = 10.54 ms), substantial signal decrease was observed for higher nanoparticle concentrations; as expected, with increasing concentration, the signal decrease was observed in the T2-weighted image. These MRI results were supplemented by the results of r1 relaxivity values measured at 23 °C.

4. Conclusions

In this work we presented a drug delivery system based of Gd_2O_3 nanoparticles encapsulated in porous silica matrix SBA-15 with hexagonal pore symmetry and incorporated anticancer drug 5-fluorouracil. Basic characterization was conducted including TEM and EDX, where the structure of samples and loading of nanoparticles into the pores was confirmed. Measurement of hydrodynamic size and Zeta potential provided us with information about samples colloidal stability, where at pH = 2 both samples indicated aggregation of nanoparticles due to strong dipolar interactions. Blank SBA-15 matrix at pH 7 showed an optimal ZP value (−33.8 mV), but samples with incorporated nanoparticles already showed increased negative values. The value of ZP of sample with nanoparticles and the drug (Gd_2O_3/SBA-15/5FU) skyrocketed up to −85 mV, which could be caused by the modification of the surface charge by a non-polar agent that contained the drug.

The magnetic properties of the studied drug-delivery system are completely caused by the magnetic behavior of the Gd_2O_3 nanoparticles. The paramagnetic behavior in the studied sample Gd_2O_3/SBA-15/5FU was observed from temperature and field dependence of magnetization. Since Gd^{3+} ions are localized, their mutual ferromagnetic exchange interactions are suppressed and the system exhibit paramagnetism. The field dependence of isothermal magnetization obtained at 2 K shows the shape of hysteresis and reaches very high magnetization. This is a signature of paramagnetic behavior. Its origin stems from the thermal randomization of Gd^{3+} magnetic spins. The negative Curie–Weiss temperature of $\Theta = -2.04$ K points to antiferromagnetic ordering mediated by

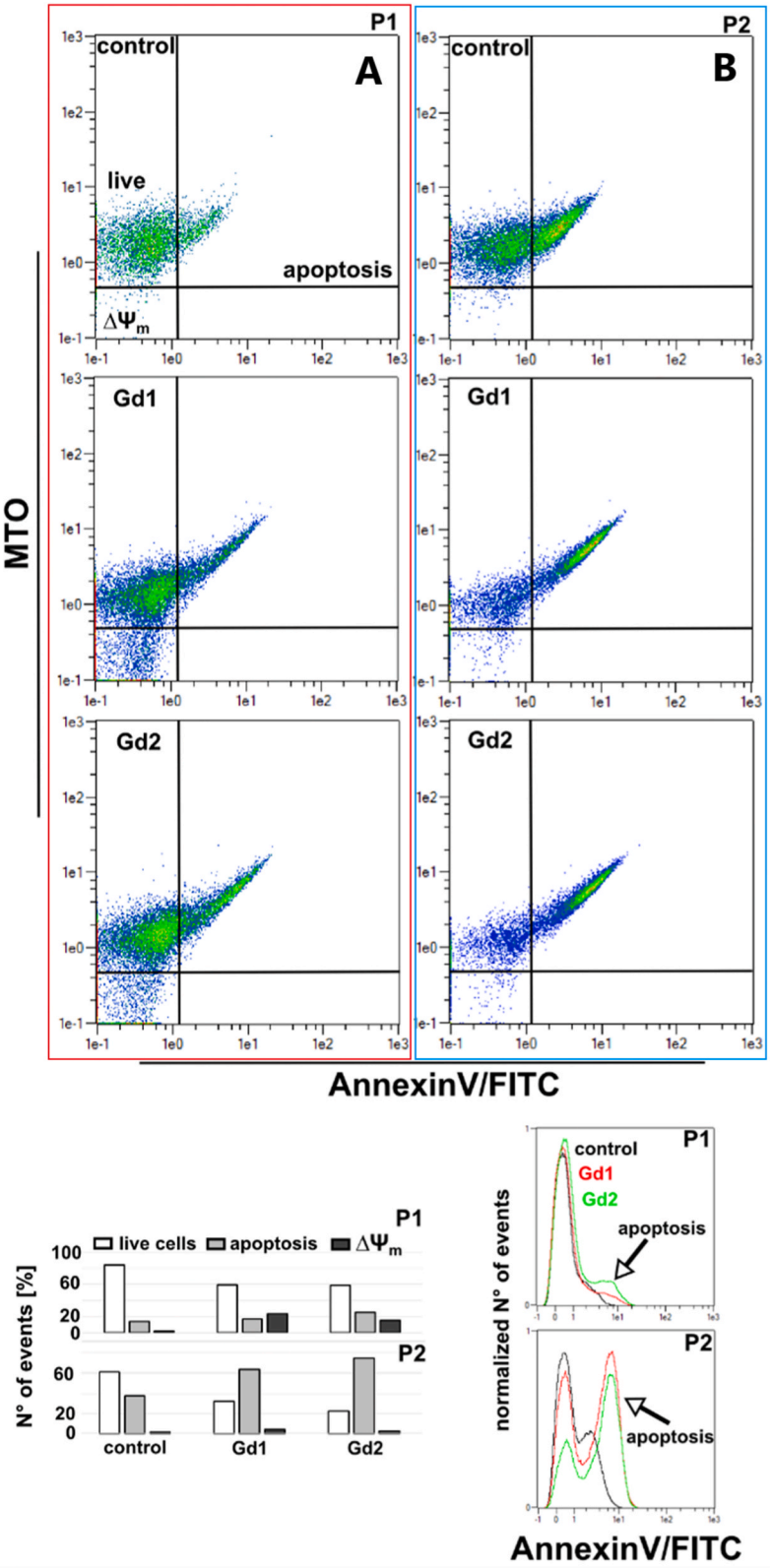

Fig. 12. Flow cytometric analysis of cell populations (P1 and P2) in the absence and in the presence of Gd1 (Gd_2O_3/SBA-15) and Gd2 (Gd_2O_3/SBA-15/5FU) nanoparticles.

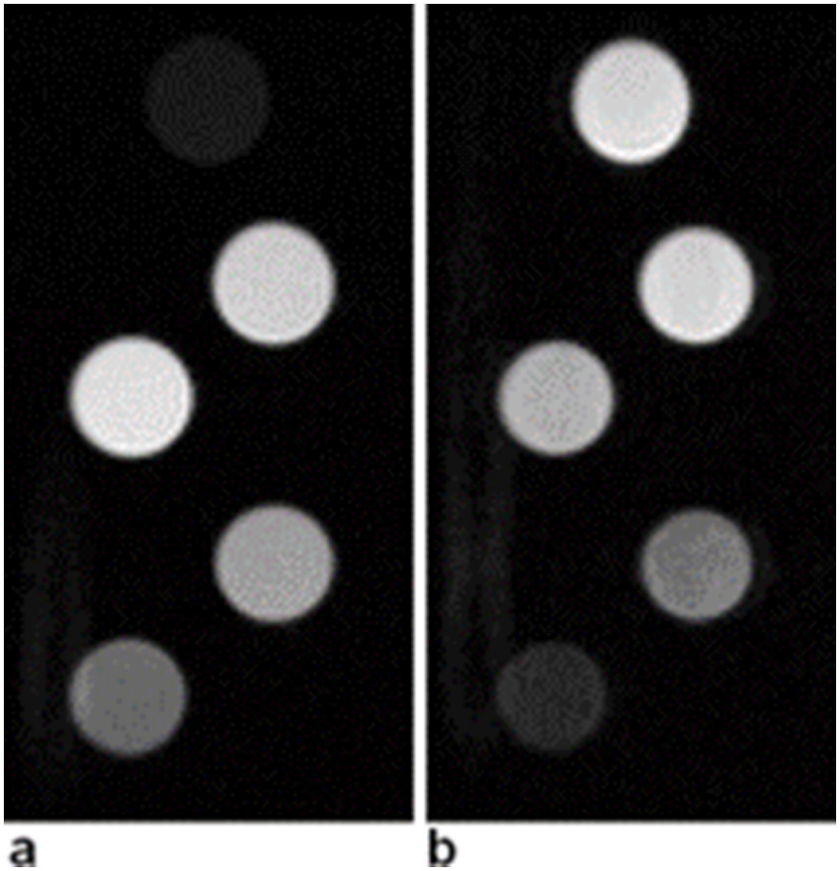

Fig. 13. MRI of the phantom containing test tubes with different nanoparticle concentrations. From top: 0 mM (control sample), 1 mM, 2 mM, 5 mM, 10 mM Gd; a) a T1-weighted image, b) a T2-weighted image.

superexchange interactions between the neighboring Gd^{3+} ions at very low temperature. The super-exchange interaction among the nearest Gd^{3+} ions mediates the observed antiferromagnetic ordering. Based on magnetic behavior with a high portion of unpaired 4f electrons, we can assume that the studied nanocomposite will have a suitable performance as a magnetic resonance imaging contrast agent (CA) for MRI cancer diagnostics.

From the cytotoxicity observations was concluded that nanocomposite with anticancer drug (Gd_2O_3/SBA-15/5FU) showed toxic behavior towards studied cells (human glioma cells U87 MG and human breast cancer cell line SK-BR 3), unlike nanocomposite without drug (Gd_2O_3/SBA-15) that was non-toxic. MTT showed that production of formazan in U87 MG cells incubated with Gd_2O_3/SBA-15 was minimally affected (20% decrease), but the significance of its influence increased with time (72 h) and concentration (100 μl/ml). In contrary, application of Gd_2O_3/SBA-15/5FU nanoparticles resulted in significant decrease in formazan production. Drug 5-FU loaded in Gd_2O_3/SBA-15/5FU was released in cells and significantly affected cell morphology and viability. Granular shape of the cells refers to cell death.

Presented drug delivery system was designed to minimalize negative effects of Gd nanoparticles and drug 5-FU due to their encapsulation into biocompatible silica matrix, so the Gd^{3+} ions are more stable (in comparison to chelates), lower therapeutic dose of 5-FU is needed and its prolongated release from silica pores was also confirmed. This drug delivery systems overall have potential to minimize toxic effects on healthy cells, because the drug is delivered and released at the desired place, so they are suitable for therapy and can be utilised also for diagnostics of the tumors. As was demonstrated from MR relaxivity measurements, the nanoparticles provided also superb T1 contrast in MR images even at low concentrations, thus system can be considered as appropriate theranostic agent.

Data availability statement

Data will be available on request.

CRediT authorship contribution statement

Jaroslava Szűcsová: Data curation, Formal analysis, Investigation, Writing – original draft. **Adriana Zeleňáková:** Conceptualization, Funding acquisition, Project administration, Supervision, Writing – original draft, Writing – review & editing. **Eva Beňová:** Data curation, Investigation, Methodology. **Ľuboš Nagy:** Data curation, Formal analysis, Investigation, Validation, Visualization. **Martin Orendáč:** Supervision. **Veronika Huntošová:** Data curation, Formal analysis, Investigation, Methodology. **Mária Šoltésová:** Data curation, Formal analysis, Investigation, Methodology, Software. **Jaroslav Kohout:** Conceptualization, Data curation, Methodology, Project administration, Supervision. **Vít Herynek:** Data curation, Formal analysis, Software, Supervision, Visualization, Writing – original draft. **Vladimír Zeleňák:** Conceptualization, Funding acquisition, Supervision.

Declaration of competing interest

The authors declare the following financial interests/personal relationships which may be considered as potential competing interests:Adriana Zelenakova reports financial support was provided by Slovak Research and Development Agency.

Acknowledgement

We would like to thank the Slovak Research and Development Agency under the contracts APVV-20-0512, APVV-SK-SRB-21-0056, APVV-20-0072, by the VEGA No. 1/0829/21 and GAČR 21-02550S for financial supports. This work was also partially supported by the Operational Programme Integrated Infrastructure, project "NANOVIR", ITMS: 313011AUW7, co-funded by ERDF. We would like to thank Dr. V. Girman for realization of TEM measurements.

References

[1] D.V. Bhalani, B. Nutan, A. Kumar, A.K. Singh Chandel, Bioavailability Enhancement techniques for poorly aqueous soluble drugs and therapeutics, Biomedicines 10 (9) (2022), https://doi.org/10.3390/biomedicines10092055, 2055.
[2] M. Kolter, M. Wittmann, M. Köll-Weber, R. Süss, The suitability of liposomes for the delivery of hydrophobic drugs - a case study with curcumin, Eur. J. Pharm. Biopharm. 140 (2019) 20–28, https://doi.org/10.1016/j.ejpb.2019.04.013.
[3] W. Xu, L. Huang, W. Jin, et al., Encapsulation and release behavior of curcumin based on nanoemulsions-filled alginate hydrogel beads, Int. J. Biol. Macromol. 134 (2019) 210–215, https://doi.org/10.1016/j.ijbiomac.2019.04.200.
[4] O. Afzal, A.S.A. Altamimi, et al., Nanoparticles in drug delivery: from history to therapeutic applications, Nanomaterials 12 (24) (2022) 4494, https://doi.org/10.3390/nano12244494.
[5] A. Eftekhari, C. Kryschi, D. Pamies, et al., Natural and synthetic nanovectors for cancer therapy, Nanotheranostics 7 (3) (2023) 236–257, https://doi.org/10.7150/ntno.77564.
[6] W. Qian, H. Wang, J. Chen, Y. Kong, Spherical V-Fe-MCM-48: the synthesis, characterization and hydrothermal stability, Materials 8 (2015) 1752–1765, https://doi.org/10.3390/ma8041752.
[7] L. Cai, Y. Huang, Y. Duan, et al., Schiff-base silver nanocomplexes formation on natural biopolymer coated mesoporous silica contributed to the improved curative effect on infectious microbes, Nano Res. 14 (2021) 2735–2748, https://doi.org/10.1007/s12274-020-3279-6.
[8] I.S. Ahmadov, A.A. Bandaliyeva, A.N. Nasibova, F.V. Hasanova, R.I. Khalilov, The synthesis of the silver nanodrugs in the medicinal plant Baikal skullcap (Scutellaria baicalensis georgi) and their antioxidant, antibacterial activity, Advances in Biology & Earth Sciences 5 (No.2) (2020) 103–118.
[9] M. Abd Elkodous, G.S. El-Sayyad, I.Y. Abdelrahman, et al., Therapeutic and diagnostic potential of nanomaterials for enhanced biomedical applications, Colloids Surf. B Biointerfaces 180 (2019) 411–428, https://doi.org/10.1016/j.colsurfb.2019.05.008.
[10] Z. Xu, L. Cai, H. Jiang, et al., Real-time cell analysis of the cytotoxicity of a pH-responsive drug-delivery matrix based on mesoporous silica materials functionalized with ferrocenecarboxylic acid, Anal. Chim. Acta (2018), https://doi.org/10.1016/j.aca.2018.11.017.
[11] Y. Song, P. Zhu, Y. Wu, et al., Epsilon-poly-l-lysine decorated ordered mesoporous silica contributes to the synergistic antifungal effect and enhanced solubility of a lipophilic drug, Mater. Sci. Eng. C 99 (2019) 231–240, https://doi.org/10.1016/j.msec.2019.01.077.
[12] Reema Narayan, Shivaprasad Gadag, Sanjay Garg, Y. Usha, Nayak, understanding the effect of functionalization on loading capacity and release of drug from mesoporous silica nanoparticles: a computationally driven study, ACS Omega 7 (10) (2022) 8229–8245, https://doi.org/10.1021/acsomega.1c03618.
[13] K. Trzeciak, A. Chotera-Ouda, I.I. Bak-Sypien, M.J. Potrzebowski, Mesoporous silica particles as drug delivery systems-the state of the art in loading methods and the recent progress in analytical techniques for monitoring these processes, Pharmaceutics 13 (7) (2021) 950, https://doi.org/10.3390/pharmaceutics13070950.
[14] M. Vallet-Regí, Our contributions to applications of mesoporous silica nanoparticles Author links open overlay panel, Acta Biomater. 137 (2022) 44–52, https://doi.org/10.1016/j.actbio.2021.10.011.
[15] Y. Zhang, J. Cheng, N. Li, et al., A versatile theranostic nanoplatform based on mesoporous silica, Mater. Sci. Eng., C 98 (2019) 560–571, https://doi.org/10.1016/j.msec.2019.01.004.
[16] J. Lux, A.D. Sherry, Advances in gadolinium-based MRI contrast agent designs for monitoring biological processes in vivo, Curr. Opin. Chem. Biol. 45 (2018) 121–130, https://doi.org/10.1016/j.cbpa.2018.04.006.
[17] A. Narmani, B. Farhood, H. Haghi-Aminjan, et al., Gadolinium nanoparticles as diagnostic and therapeutic agents: their delivery systems in magnetic resonance imaging and neutron capture therapy, J. Drug Deliv. Sci. Technol. 44 (2018) 457–466, https://doi.org/10.1016/j.jddst.2018.01.011.
[18] Y. Dai, C. Wu, S. Wang, et al., Comparative study on in vivo behavior of PEGylated gadolinium oxide nanoparticles and Magnevist as MRI contrast agent, Nanomedicine 14 (2) (2018) 547–555, https://doi.org/10.1016/j.nano.2017.12.005.
[19] S.L. Ho, H. Cha, I.T. Oh, et al., Magnetic resonance imaging, gadolinium neutron capture therapy, and tumor cell detection using ultrasmall Gd_2O_3 nanoparticles coated with polyacrylic acid-rhodamine B as a multifunctional tumor theragnostic agent, RSC Adv. 8 (23) (2018) 12653–12665, https://doi.org/10.1039/C8RA00553B.
[20] R. Marasini, T.D. Thanh Nguyen, S. Aryal, Integration of gadolinium in nanostructure for contrast enhanced-magnetic resonance imaging, Wiley Interdiscip Rev Nanomed Nanobiotechnol 12 (1) (2020), e1580, https://doi.org/10.1002/wnan.1580.
[21] S. Iraji, F. Ganji, L. Rashidi, Surface modified mesoporous silica nanoparticles as sustained-release gallic acid nano-carriers, J. Drug Deliv. Sci. Technol. 47 (2018) 468–476, https://doi.org/10.1016/j.jddst.2018.08.008.
[22] Xiaoxiao Sun, Chao Liu, et al., pH-sensitive ZnO/carboxymethyl cellulose/chitosan bio-nanocomposite beads for colon-specific release of 5-fluorouracil, Int. J. Biol. Macromol. 128 (2019) 468–479, https://doi.org/10.1016/j.ijbiomac.2019.01.140.
[23] A. Zeleňáková, P. Hrubovčák, A. Berkutova, et al., Gadolinium-oxide nanoparticles for cryogenic magnetocaloric applications, Sci. Rep. 12 (1) (2022), https://doi.org/10.1038/s41598-022-06132-8.

[24] V. Zeleňák, A. Zeleňáková, O. Kapusta, P. Hrubovčák, V. Girman, J. Bednarčík, Fe_2O_3 and Gd_2O_3 nanoparticles loaded in mesoporous silica: insights into influence of NPs concentration and silica dimensionality, RSC Adv. 9 (7) (2019) 3679–3687, https://doi.org/10.1039/C8RA05576A.
[25] A. Zelenakova, P. Hrubovčák, O. Kapusta, V. Zeleňák, V. Franco, Large magnetocaloric effect in fine Gd_2O_3 nanoparticles embedded in porous silica matrix, Appl. Phys. Lett. 109 (2016), 122412, https://doi.org/10.1063/1.4963267.
[26] A. Fatima, M.W. Ahmad, et al., Recent advances in gadolinium based contrast agents for bioimaging applications, Nanomaterials 11 (2021) 2449, https://doi.org/10.3390/nano11092449.
[27] S. Marasini, H. Yue, et al., Polyaspartic acid-coated paramagnetic gadolinium oxide nanoparticles as a dual-modal T1 and T2 magnetic resonance imaging contrast agent, Appl. Sci. 11 (17) (2021) 8222, https://doi.org/10.3390/app11178222.
[28] V. Zeleňák, A. Zeleňáková, J. Kováč, Insight into surface heterogenity of SBA-15 silica: oxygen related defects and magnetic properties, Colloids Surf. A Physicochem. Eng. Asp. 357 (1–3) (2010) 97–104, https://doi.org/10.1016/j.colsurfa.2010.01.001.